# Phase locking of spin-torque nano-oscillator pairs with magnetic dipolar coupling

Hao-Hsuan Chen,[1] Ching-Ming Lee,[2,*] Zongzhi Zhang,[1,†] Yaowen Liu,[3,‡] Jong-Ching Wu,[4]
Lance Horng,[4] and Ching-Ray Chang[5]

[1]*Shanghai Ultra-Precision Optical Engineering Center, Department of Optical Science and Engineering, Fudan University,
Shanghai 200433, People's Republic of China*
[2]*Graduate School of Materials Science, National Yunlin University of Science and Technology, Douliou, 64002, Taiwan,*
[3]*School of Physics Science and Engineering, Tongji University, Shanghai 200092, People's Republic of China*
[4]*Department of Physics, National Changhua University of Education, Changhua 500, Taiwan*
[5]*Department of Physics, National Taiwan University, Taipei 10617, Taiwan*

A spin-torque nanopillar oscillator (STNO) that combines a perpendicular-to-plane polarizer (PERP) with an in-plane magnetized free layer is a good candidate for phase locking, which opens a potential approach to enhancement of the output power of STNOs. In this paper, the magnetic dipolar coupling effect is used as the driving force to synchronize two STNOs. We develop an approximation theory for synchronizing two identical and nonidentical pairs of PERP STNOs, by which the critical current of synchronization, dipolar coupling strength, phase-locking transient time, and frequency can be analytically predicted. These predictions are further confirmed by macrospin and micromagnetic simulations. Finally, we show the phase diagrams of the phase locking as a function of applied current and separation between two STNOs.

## I. INTRODUCTION

A spin-polarized current can be used to excite persistent magnetization oscillations in a nanomagnet through the spin-transfer torque (STT) effect [1,2]. Such STT-driven magnetic precession has attracted considerable attention because of both the fundamental interest for studying nanoscale magnetic dynamics and the applications in the frequency tunable microwave oscillators [3], which can be used in telecommunications, microwave signal processors, and microwave field detectors [4–9]. The frequency of STT oscillators can be tuned by the strength of magnetic fields or current. However, the present output power of a single spin-valve spin-torque nanopillar oscillator (STNO) is typically in the range of picowatts to nanowatts [10,11], which is still too weak for any practical applications.

Increasing output power of a STNO is essential for successful adaptation of the STT excitation scheme for advanced microwave oscillators. Several ways to enhance the output signals have been reported. For example, using a magnetic tunnel junction (MTJ) to replace the spin valve element can increase the output power to microwatt level [12–14]; using the perpendicular-to-plane magnetized layer as the spin polarizer of STNOs can excite large angle out-of-pane (OP) precession for enhancement of the power output [15–21]. Up to now, a single STT device has been significantly optimized, but the output power still cannot reach the required milliwatts.

Another promising approach to increasing the emitted power has been suggested by using the phase-locking mode of an array of STNOs through the synchronization technique. This is a very challenging issue due to the strongly nonlinear property of STNOs [22,23]. A phase-locking experiment has

been reported in spin-torque devices with multiple nanocontacts [24–31], in which the magnetization in all the nanocontact regions can be locked in the same phase via propagating spin-waves [32–34]. Alternatively, the phase locking by using the coupled electrical circuits has also been proposed in an array of STNO nanopillars electrically connected in series or in parallel [35–37]. Recently, a third scheme using the magnetic dipolar coupling effect as the driving source of synchronization has been demonstrated in nanopillars that combines the out-of-plane magnetized polarizer and the in-plane magnetized free layer namely, perpendicular-to-plane polarizer (PERP) STNO [19,38,39]. Additionally, another kind of oscillator based on the spin Hall effect (SHE), i.e. spin Hall oscillators (SHOs), have been also reported recently [40–45]. Moreover, the synchronization of vortex-based nonuniformly magnetized STNOs in a horizontal array has also been reported [46–49]. Among these synchronization schemes, the scheme using the magnetic dipolar effect displays special features [38,47,48]: First, the dipolar coupling among STNOs with nanopillar structure is an intrinsic property, so that it does not need any other external sources such as external microwave field or a special design of resistor-inductor-capacitor (RLC) circuit to assist synchronization. Second, unlike the scheme employing a propagating spin wave [31], in which the phase-locking mode can be either in phase or antiphase, depending on the intercontact distance and current strength, the magnetization phase-locking state induced by the dipolar interaction is very stable, and the antiphase mode is independent of the current and separation between neighboring STNOs [38].

In this paper, we present a phase-locking scheme to synchronize two horizontally arranged PERP STNOs through the dipolar coupling effect of the free layers. The paper is organized as follows: In Sec. II, we develop a theory for synchronizing two identical and nonidentical pairs of PERP STNOs. The pairs are horizontally arranged. The sufficient and necessary parametric conditions for the synchronization are addressed, based on the assumption of strong demagnetization

---
*cmlee@yuntech.edu.tw
†zzzhang@fudan.edu.cn
‡yaowen@tongji.edu.cn

energy and the dipolar coupling approximation with a single domain model. We analytically predict the critical current, critical dipolar coupling strength, as well as the phase-locking frequency and phase-locking transient time. In Sec. III, we perform both macrospin and micromagnetic simulations. The simulation results are consistent with our analytical predictions, by showing the time evolution of the phase difference, spectrum analysis of the synchronization oscillations, the current range, and the separation distance between the two synchronized STNOs. We also show parameter diagrams of phase locking. Finally, a brief summary and discussions are given in Sec. IV. Appendix A provides details of the calculation of magnetic dipolar interaction between two circular, uniformly magnetized discs, and Appendix B presents an approximation theory using a low-energy orbit to derive the Newton-like Eq. (5).

## II. MODEL AND THEORETICAL FRAMEWORK

As a model system, we consider here a pair of STNOs shown in Fig. 1. The bottom layer is the spin polarizer layer (P) whose magnetization is fixed along the perpendicular-to-plane direction. The top layer is supposed to be etched down to the nonmagnetic metal layer. The free layers (F1 and F2) of the two nanopillars are separated by an edge-to-edge distance $d_{ee}$. We assume that the free layer has a quasiuniform in-plane magnetization due to its small size. A dc electric current separately flows from the bottom layer to the two free layers F1 and F2. We assume that the two pillars have the same amount of injected current (each one has $-I$). When the current strength is larger than a critical value, the current-induced STT effect will drive the two free-layer magnetizations into a precessional state [15,21]. Owing to the magnetic dipolar interaction between the two free layers, the two STNOs can oscillate synchronously under certain conditions.

The magnetization dynamics of the two free layers can be described by the Landau-Lifshitz-Gilbert (LLG) equation including the STT term [19,50–52]

$$\frac{d\mathbf{m}_i}{d\tau} = -\left(\nabla_{\mathbf{m}_i} G\right) \times \mathbf{m}_i + \alpha\left(\mathbf{m}_i \times \frac{d\mathbf{m}_i}{d\tau}\right) - a_J(\mathbf{m}_i)[\mathbf{m}_i \times (\mathbf{m}_i \times \mathbf{p})], \quad (1)$$
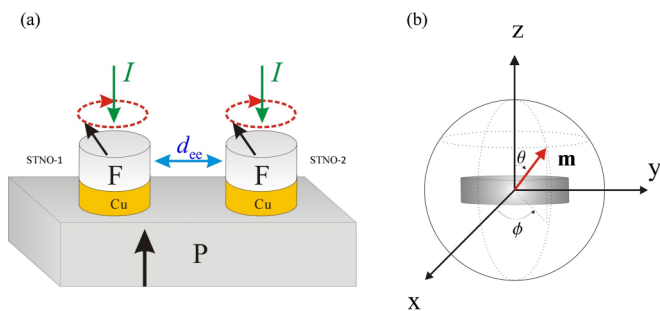


FIG. 1. (a) Sketch of a horizontal array containing two PERP STNOs. P denotes the spin polarizer layer (i.e. the fixed layer), and F denotes the free layer. (b) The unit vector $\mathbf{m}$ of free layer magnetization is illustrated in the polar coordinate representation $(\theta, \phi)$.

where the subscript $i(=1, 2)$ is used to distinguish the two nanopillars. Here, $\mathbf{m} = \mathbf{M}/M_s$ is the unit vector of the free-layer magnetization, $M_s$ is the saturation magnetization, and $\tau = (4\pi M_s \gamma)t$ is the scaled time, with $\gamma = 1.76 \times 10^7 \, \mathrm{Oe}^{-1} \cdot \mathrm{s}^{-1}$ being the gyromagnetic ratio. Also, $G(\mathbf{m})$ is the total energy density of the free layer which has been normalized by $4\pi M_s^2$. Further, $\alpha$ is the Gilbert damping constant. The third term on the right side of Eq. (1) is the STT term, in which $\mathbf{p}$ is a unit vector of the polarizer magnetization along the $z$ direction, and $a_J(\mathbf{m}_i) = A_J(\mathbf{m}_i)(4\pi M_s \gamma)^{-1} = a_{J0}\varepsilon(\theta_i, P_i, \Lambda_i)$ is the scaled-down STT strength in which $A_J(\mathbf{m}_i) = A_{J0}\varepsilon(\theta_i, P_i, \Lambda_i) = (\gamma \hbar J/2eM_s d)\varepsilon(\theta_i, P_i, \Lambda_i)$. Here, $J$ is the injected current density, $P$ is the spin polarization, $d$ is the free-layer thickness, and $\theta$ is the angle between the magnetization vectors of the free layer and the polarizer layer. Also, $\varepsilon(\theta_i, P_i, \Lambda_i) = P_i \Lambda_i^2/[(\Lambda_i^2 + 1) + (\Lambda_i^2 - 1)\cos\theta_i](i = 1, 2)$ is the angular dependence factor of the Slonczewski STT [1], in which $P$ and $\Lambda$ are dimensionless quantities which determine the spin-polarization efficiency.

In the spherical coordinates $(\theta, \phi)$ [see Fig. 1(b)], the total energy density $G(\mathbf{m})$ is given by the sum of the demagnetization energy, uniaxial anisotropic energy, and magnetic dipolar interaction energy

$$G_{dem}(\theta_1, \theta_2) = \frac{1}{2}\sum_{i=1}^{2}m_{zi}^2 = \frac{1}{2}\sum_{i=1}^{2}\cos^2\theta_i, \quad (2)$$

$$G_u(\theta_1, \phi_1, \theta_2, \phi_2) = \frac{k}{2}\sum_{i=1}^{2}m_{xi}^2 = \frac{k}{2}\sum_{i=1}^{2}\sin^2\theta_i\sin^2\phi_i, \quad (3)$$

$$G_{dip}(\theta_1, \phi_1, \theta_2, \phi_2) = A_{disc}(d_{ee})[3(\mathbf{m}_1 \cdot \mathbf{r})(\mathbf{m}_2 \cdot \mathbf{r}) - \mathbf{m}_1 \cdot \mathbf{m}_2]$$
$$= A_{disc}(d_{ee})[\sin\theta_1\sin\theta_2(\sin\phi_1\sin\phi_2 - 2\cos\phi_1\cos\phi_2) + \cos\theta_1\cos\theta_2], \quad (4)$$

where $k$ is the uniaxial anisotropy constant, either a magnetic anisotropy or a shape anisotropy. The easy-axis of the anisotropy is along the $x$-axis direction. Here, $A_{disc}(d_{ee})$ is the strength coefficient of the dipolar field that describes the magnetostatic interaction effect between the two nanopillars, and $d_{ee}$ is the edge-to-edge separation distance. The vector $\mathbf{r}$ is a unit vector of the displacement between two magnetic dipoles. In order to improve the accuracy of our approximation, the dipolar interaction in Eq. (4) is treated as the interaction between two circular uniformly magnetized discs (for details see Appendix A). The strength $A_{disc}(d_{ee})$ is more realistic than the point dipoles strength $A_{point}(d_{ee})$ due to the finite size effect [53]. We find that, when the distance $d_{ee}$ is smaller than 30 nm, then $A_{disc}(d_{ee})$ is significantly larger than $A_{point}(d_{ee})$, see Appendix A.

In order to get proper parameters and gain insight into the phase-locking behavior, an approximation theory is introduced here. We assume that the free-layer magnetization is approximately suppressed in the easy plane with $\theta_i \sim \pi/2$ due to the strong demagnetizing field. In this case, the system executes low-energy orbits, and the total magnetic energy density of the system can be approximately written as $|G| \sim k > |G_{dip}| \sim A_{disc}(d_{ee})$. These low-energy orbits
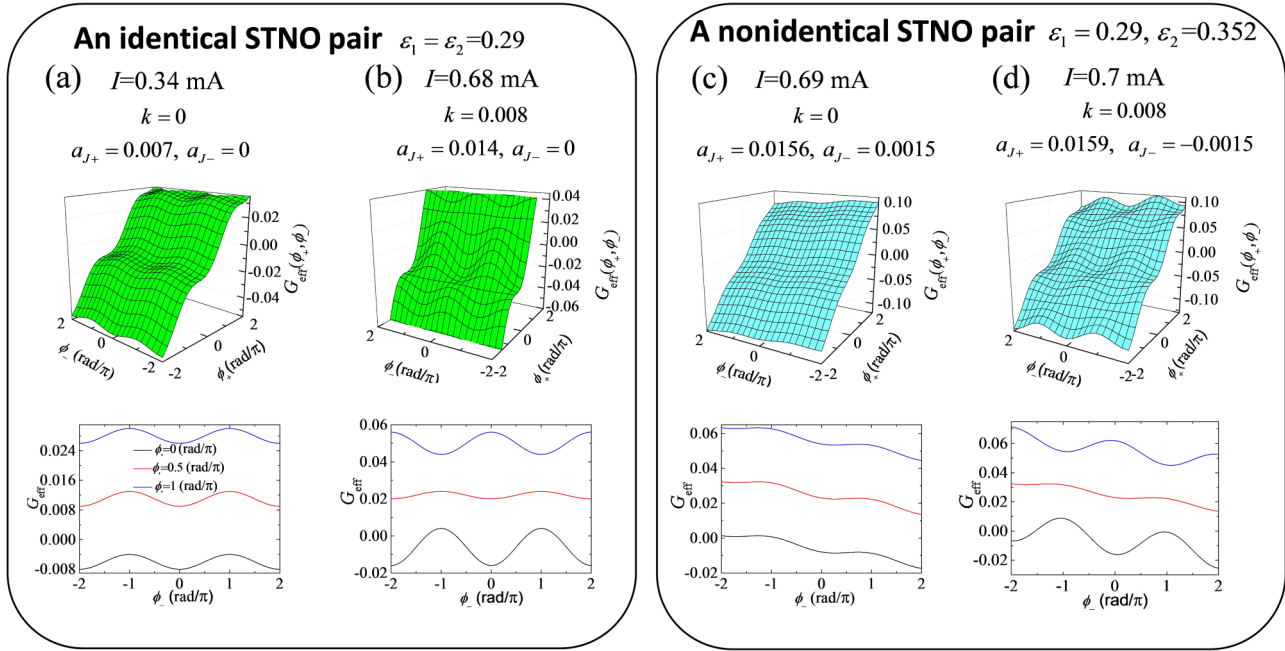
FIG. 2. Effective potential energy $G_{\text{eff}}(\phi_+,\phi_-)$ for the (a) and (b) identical STNO pair and (c) and (d) nonidentical STNO pair at different uniaxial anisotropy $k$ and different current $I$. Three cross-sections taken at $\phi_+ = 0, \pi/2, \pi$ are shown in the corresponding bottom panels of each figure. Here, $d_{\text{ee}} = 20$ nm, and $A_{\text{disc}}(d_{\text{ee}}) = 0.002$. All parameters are marked in the figures.

satisfy $[\theta_i(\tau), \phi_i(\tau)] = [\pi/2 + \delta\theta_i(\tau), \phi_i(\tau)](i = 1, 2)$, where $|\delta\theta_i| \sim \sqrt{k}$. If the damping constant and the STT strength satisfy Eq. (B13), then Eq. (1) can be rewritten as a pair of Newton-like equations (see Appendix B for details)

$$\ddot{\phi}_1 + \alpha\dot{\phi}_1 = A_{\text{disc}}(d_{ee})[-\sin(\phi_1 + \phi_2) - \sin\phi_1\cos\phi_2]$$
$$- \frac{k}{2}\sin 2\phi_1 + a_{J1}\left(\theta_1 = \frac{\pi}{2}\right), \quad (5a)$$

$$\ddot{\phi}_2 + \alpha\dot{\phi}_2 = A_{\text{disc}}(d_{ee})[-\sin(\phi_1 + \phi_2) - \cos\phi_1\sin\phi_2]$$
$$- \frac{k}{2}\sin 2\phi_2 + a_{21}\left(\theta_2 = \frac{\pi}{2}\right), \quad (5b)$$

where the effective force is dominated by the dipolar interaction term (the first term of the right-hand side), the uniaxial anisotropy (the second term), and the STT term (the third term). For simplicity, by using a new set of variables formed by the phase sum $\phi_+ = \phi_1 + \phi_2$ and the phase difference $\phi_- = \phi_1 - \phi_2$, we rewrite Eqs. (5a) and (5b) as

$$\frac{d^2\phi_+}{d\tau^2} + \alpha\frac{d\phi_+}{d\tau} = -\frac{\partial G_{\text{eff}}(\phi_+,\phi_-)}{\partial\phi_+}, \quad (6a)$$

$$\frac{d^2\phi_-}{d\tau^2} + \alpha\frac{d\phi_-}{d\tau} = -\frac{\partial G_{\text{eff}}(\phi_+,\phi_-)}{\partial\phi_-}, \quad (6b)$$

where the effective potential energy is now given by

$$G_{\text{eff}}(\phi_+,\phi_-) = A_{\text{disc}}(d_{ee})(-3\cos\phi_+ - \cos\phi_-)$$
$$- k\cos\phi_-\cos\phi_+ + a_{J+}\phi_+ + a_{J-}\phi_-. \quad (7)$$

Here, $a_{J+} \equiv a_{J1} + a_{J2}$ and $a_{J-} = a_{J1} - a_{J2}$.

### A. An identical STNO pair

According to the design shown in Fig. 1, the STT strength is the same for two identical PERP STNOs, that is, $a_{J-} = 0$ and $a_{J+} = 2a_J$. From Eq. (6a) with Eq. (7), by setting $|\partial G_{\text{eff}}/\partial\phi_+| > 0$, we obtain $|a_{J+}| > 3A_{\text{disc}}(d_{ee}) + k$, and under this condition, all equilibria of $G_{\text{eff}}$ along the $\phi_+$-axis direction are eliminated (Fig. 2). This condition indicates that there exists a critical STT strength (or critical current) to drive the two STNOs into a steady OP precessional state

$$|a_{J1,c}| = |a_{J2,c}| = (1/2)|a_{J+,c}| = (1/2)[3A_{\text{disc}}(d_{ee}) + k]. \quad (8a)$$

At $d_{\text{ee}} = 20$ nm, we have $A_{\text{disc}}(d_{ee}) = 0.002$ (Fig. 10 in Appendix A). In the absence of uniaxial anisotropy (i.e. $k = 0$), we further get the critical STT strength $a_{J+,c} = 0.006$ and the current $I_c = 0.29$ mA. Similarly, in the presence of uniaxial anisotropy ($k = 0.008$), we have $a_{J+,c} = 0.014$ and $I_c = 0.68$ mA.

Note that, when the current is larger than the critical value given by Eq. (8a), the two STNOs can be driven into a precessional state, but the precession may not be synchronous. Therefore, the synchronization or phase-locking state requires additional conditions. From Eqs. (6b) and (7), by setting $\partial G_{\text{eff}}/\partial(\phi_-) = 0$ and $\partial^2 G_{\text{eff}}/\partial(\phi_-)^2 > 0$, the condition for $\phi_- = 0$ as the only stable equilibrium point in the range of $\phi_+ \in [0, 2\pi]$ can be derived

$$A_{\text{disc}}(d_{ee}) > k. \quad (8b)$$

We would like to emphasize that Eq. (8b) guarantees that the two free layers of the coupled system always evolve into a final state with a stable phase difference beginning with an arbitrary initial state. If Eqs. (8a) and (8b) are simultaneously satisfied, Eqs. (6a) and (6b) can be reduced to a single equation

of motion

$$\ddot{\phi} + \alpha\dot{\phi} = -(1/2)[3A_{\text{disc}}(d_{\text{ee}}) + k]\sin 2\phi - a_J, \quad (9)$$

where $\phi \equiv (1/2)\phi_+ = \phi_1 = \phi_2$ and $a_J \equiv (1/2)a_{J+} = a_{J1} = a_{J2}$. It should be noticed that Eq. (9) has the same form as Eq. (5) for a single oscillator, but the anisotropy energy is enhanced by including the dipolar coupling term $3A_{\text{disc}}(d_{\text{ee}})$. Therefore, we conclude that Eqs. (8a) and (8b) are the necessary and sufficient conditions for the phase locking of magnetization precession of two nano-oscillators. On the other hand, note from Eqs. (8) and (8b) that the anisotropy $k$ can raise the threshold values of the dipolar strength $A_{\text{disc}}$, and of the critical spin-transfer strength $a_{Jc}$ as well. This analytical result suggests that the reduction of anisotropy is a possible way to reduce the critical current as well as to enhance the stability of a phase-locked array of STNOs.

In order to obtain a qualitative insight into Eq. (8), we regard the dipolar coupled STNOs pair as an effective Newton-like particle moving on the energy surface $G_{\text{eff}}$. As shown in Fig. 2(a), in the absence of uniaxial anisotropy when the current $I = 0.34$ mA (larger than $I_c = 0.29$ mA at $k = 0$), the energy surface will be tilted along $-\phi_+$ direction by the sum of the STT strengths $a_{J+}$. Because there are no stable equilibrium points along the $\phi_+$ axis, the particle will move downward along the $-\phi_+$ direction with an average terminal velocity $|\langle\dot{\phi}\rangle|_\tau = |a_{J+}|/\alpha$. Furthermore, the dipolar coupling creates stable equilibrium points at $\phi_- = 0$ on the energy surface. The barrier height between the local equilibria along the $\phi_-$ axis is $A_{\text{disc}}(d_{\text{ee}})$, as is shown in the lower panel of Fig. 2(a). Due to energy dissipation, the particle will eventually move downward along the ditch from any initial state with the average terminal velocity $|a_{J+}|/\alpha$, indicating that the two STNOs precess in phase. In the presence of uniaxial anisotropy, as shown in Fig. 2(b), besides the elevation of the critical current, also the cross-section shape of the ditch on the energy surface is changed with $\phi_+$ [see the lower panel of Fig. 2(b)], meaning that uniaxial anisotropy is certainly detrimental to phase locking.

### B. A nonidentical STNO pair

Now we consider two nonidentical PERP STNOs. The nonidentical property may be caused by asymmetric STT strengths (that is, $a_{J-} \neq 0$) or by other parameters (for example, shape difference). Similar to the identical case, by analytically setting $|\partial G_{\text{eff}}/\partial\phi_+| > 0$, $\partial G_{\text{eff}}/\partial(\phi_-) = 0$, and $\partial^2 G_{\text{eff}}/\partial(\phi_-)^2 > 0$, one can obtain the phase-locking conditions as the following form:

$$|a_{J+}| > 3A_{\text{disc}}(d_{\text{ee}}) + k, \quad (10a)$$

$$A_{\text{disc}}(d_{\text{ee}}) > k, \quad (10b)$$

and

$$|a_{J-}| < A_{\text{disc}}(d_{\text{ee}}) - k. \quad (10c)$$

Here, Eq. (10c) guarantees the difference of STT strengths is not so strong as to destroy the phase-locking state. Additionally, from the Eq. (10a), we can estimate that the critical currents $I_c$ in the absence and presence of the energy $k$ are 0.26 and 0.62 mA, respectively.

Assuming that the edge-to-edge distance $d_{\text{ee}}$ is approximately 30 nm or less, the corresponding dipolar interaction

strength $A_{\text{disc}}(d_{\text{ee}})$ does not easily satisfy the condition of $A_{\text{disc}}(d_{\text{ee}}) > k$. This circumstance is due to the fact that, for the given value $k = 0.008$, the value of $A_{\text{disc}}(d_{\text{ee}})$ is, according to Fig. 10, smaller than $k$ unless the separation $d_{\text{ee}}$ is decreased down to 5 nm. By inserting Eq. (7) into Eq. (6b), we now obtain

$$\frac{d^2\phi_-}{d\tau^2} + \alpha\frac{d\phi_-}{d\tau} = -\sin(\phi_-)[A_{\text{disc}}(d_{\text{ee}}) + k\cos(\phi_+)] - a_{J-}, \quad (11)$$

The first term on the right-hand side of Eq. (11) is the restoring force, in which the uniaxial anisotropy $k$ actually contains a prefactor rapidly varying in time $\cos(\phi_+)$. This is because the $\phi_+$ varies faster than the growth of the phase difference $\phi_-$ when $|a_{J-}|$ is smaller than the dipolar interaction strength $A_{\text{disc}}(d_{\text{ee}})$. Thus, the terminal velocity of the phase difference $|\dot{\phi}_-| < A_{\text{disc}}(d_{\text{ee}})/\alpha$ must be smaller than that of the phase sum $|\dot{\phi}_+| > (3A_{\text{disc}}(d_{\text{ee}}) + k)/\alpha$. Here, the perturbation of anisotropy $k$ oscillates very fast compared to the phase difference change, so that the perturbation can be omitted by the approach presented below [54].

Taking a time average of $\phi_-$ in Eq. (6b) over a period of $\Delta T = 2\pi/|\dot{\phi}_-| = 2\pi A_{\text{disc}}(d_{\text{ee}})/\alpha$, one can easily find that the contribution of the time-varying part in $\phi_-$ becomes close to zero, i.e. $\langle\cos(\phi_+)\rangle_{\Delta T} \approx 0$. Therefore, the right-hand side of Eq. (6b) takes on the form $-A_{\text{disc}}(d_{\text{ee}})\sin(\phi_-) - a_{J-}$. As a consequence, a soft phase-locking condition for the nonidentical pair of PERP STNOs is obtained

$$|a_{J+}| > 3A_{\text{disc}}(d_{\text{ee}}) + k, \quad (12a)$$

$$|a_{J-}| < A_{\text{disc}}(d_{\text{ee}}). \quad (12b)$$

These two Eqs. (12a) and (12b) are supported by numerical solutions of Eqs. (6a) and (6b). When the above conditions are satisfied, Eq. (6a) for phase sum $\phi_+$ is rewritten as

$$\frac{d^2\phi_+}{d\tau^2} + \alpha\frac{d\phi_+}{d\tau} = -[3A_{\text{disc}}(d_{\text{ee}}) + k\cos\phi_{+0}]\sin\phi_+ - a_{J+}, \quad (13)$$

in which $\phi_{-0}$ is the stable, nonzero phase difference. Accordingly, the phase-locked angular velocity is given by

$$|\dot{\phi}_1| = |\dot{\phi}_2| = \frac{1}{2}\left|\frac{d(\phi_+)}{d\tau}\right| = \frac{1}{2\alpha}|a_{J+}|.$$

From the viewpoint of the Newton-like particle, in the absence of uniaxial anisotropy $k = 0$, when the current $I = 0.69$ mA is larger than the critical value 0.26 mA, the energy surface will not only be tilted along the $-\phi_+$ direction by the sum of the STT strengths $a_{J+}$, but will also be tilted along the $+\phi_-$ direction by the STT strength difference $a_{J-}$, as shown in Fig. 2(c). Thus, the position of the ditch created by dipolar coupling is shifted by $a_{J-}$ slightly away from $\phi_- = 0$, and the barrier height between the local equilibriums along the $\phi_-$ axis is smaller than $A_{\text{disc}}(d_{\text{ee}})$, implying that the phase-locking ability of dipolar coupling is weakened by negative $a_{J-}$ values [lower panel of Fig. 2(c)]. Due to the energy dissipation, the particle will eventually move downward along the new ditch from any initial state, meaning that the two STNOs precess with a small phase difference. However, similar to the identical components case, the uniaxial anisotropy still changes the stability of the local equilibrium points.

## III. NUMERICAL SIMULATIONS: RESULTS AND DISCUSSION

In order to verify the analytical model, both macrospin and full micromagnetic (FMM) simulations have been performed for a coupled PERP STNO pair with dipolar magnetic interaction. In this section, we will show the time dependence of the phase difference $\phi_-$ and the inclination angle $\theta$, the $x$ and $z$ components of the precessional magnetization, and the spectrum analysis of magnetization oscillation. Furthermore, the critical conditions for triggering phase locking of magnetization with a minimum current $I$ and a maximum edge-to-edge distance $d_{ee}$ will be discussed. The simulated parameter ranges for phase locking will be compared with the results from the approximate theory.

In this paper, both macrospin and FMM simulations are conducted. The macrosopin code is developed in our group independently, and the micromagnetic simulations are carried out by using two open micromagnetic codes, the finite element package magpar [55] and the finite difference package MuMax3 [56]. In these simulations, we assume that the STNOs have an elliptical shape with size $70 \times 60$ nm, and that the free-layer thickness $d = 3$ nm. For simplicity, we only focus on the magnetization dynamics of the free layers. The initial magnetization state is aligned along the $x$ axis (long axis of the sample) direction. The thickness of the free layer is 3 nm. Typical material parameters are used for the Co free layer [16]: $4\pi M_s = 1.09 \times 10^4$ Oe (saturation magnetization), $k = 0.008$ (in-plane uniaxial anisotropy), $A = 2.5 \times 10^{-11}$ J m$^{-1}$ (exchange stiffness constant), $\alpha = 0.02$ (Gilbert damping constant). The discretization cell size for MuMax3 is set at $1 \times 1$ nm $\times 3$ nm, while the magpar average size of tetrahedron mesh is 2 nm. The spin polarization of the left STNO is set to be $P_1 = 0.38$ and $\Lambda_1 = 1.8$. The right STNO is given by $P_2 = 0.44$, $\Lambda_2 = 2$. Without dipolar interaction, the two STNOs have different oscillation frequencies (we will show this later) due to different spin polarizations.

In this paper, the current-induced Oersted field [57] is ignored. Our calculations indicate that the maximum value of the Oersted field created by a current of 0.7 mA is $\sim$40 Oe located in the perimeter zone of an isolated nanopillar (not shown). This is a reasonable estimation for considering the Oersted fields created by current as an infinite wire. The Oersted field is therefore much smaller than other fields such as the in-plane uniaxial anisotropy field ($\sim$170 Oe) and the demagnetizing field ($\sim$1.09 $\times 10^4$ Oe). For a pair of nanopillars horizontally arranged with an edge-to-edge separation changing from 5 to 20 nm, the calculated Oersted field is further reduced down to $\sim$25 Oe due to the cancellation between the two STNOs. For this reason, the Oersted field is ignored in this paper.

### A. Synchronization of an STNO pair: Phase-locking state

First, a phase-locking state is obtained both from the analytical theory and simulations: The injected current is set to be $I = 0.8$ mA. Using the above parameter values and $\theta_1 = \theta_2 = \pi/2$, we analytically obtained the STT difference $|a_{J-}| = |a_{J1} - a_{J2}| = 0.0017$, which is smaller than the value of $A(d_{ee}) = 0.002$, meaning that the analytical condition for

phase locking shown in Eq. (12b) is satisfied. Numerically, both the macrospin and micromagnetic simulations with these parameters indicate that the phase-locking magnetization state can be achieved within several nanoseconds, as shown in the upper panels of Figs. 3(a) and 3(c). In this paper, the total simulation time is 50 ns. In order to show clearly the transient behavior, the time scales in Fig. 3 are confined to the initial several nanoseconds. The phase-locking state has a small phase difference $\phi_- = 0.23$ rad/$\pi$ in the macrospin simulation and 0.34 rad/$\pi$ in the micromagnetic simulation. This nonzero $\phi_-$ corresponds to the position shift of equilibrium points [see Fig. 2(b)], caused by $a_{J-}$. In addition, the phase-locking state of the inclination angle $\theta$ of the two STNOs has also been achieved in both simulations, as shown in the lower panel of Fig. 3(a). This phase locking of $\theta$ can also be inferred from the locking of $\dot{\phi}$, according to the conjugacy between the variables of $\phi$ and $\theta$ [see Appendix B, Eq. (B5)]. In other words, when the locking of $\phi$ occurs (that is $\dot{\phi}_1 = \dot{\phi}_2$), $\theta_1$ must be equal to $\theta_2$. Similarly, the phase locking can also be clearly seen from the magnetization plot in Cartesian coordinates, as shown in Fig. 3(b).

From Figs. 3(a)–3(c), one can see that there exists a transient state before the STNO pair synchronizes into a stable phase-locked state. The typical time order of the transient state can be theoretically estimated from the Newton-like motion equation of Eq. (6b). As mentioned before, the uniaxial anisotropy $k$ in Eq. (6b) contains a fast time-varying prefactor $\cos(\phi_+)$ which makes it possible to neglect $k$. Therefore, Eq. (6b) can be linearized close to the equilibrium point $\phi_- \sim 0$. For a small angle $\delta(\phi_-)$, we have

$$\frac{d^2\delta(\phi_-)}{d\tau^2} + \alpha\frac{d\delta(\phi_-)}{d\tau} = -\{\sqrt{[A_{disc}(d_{ee})]^2 - (a_{J-})^2}\}\delta(\phi_-).$$

The general solution $\delta(\phi_-)(\tau)$ of this equation has a decay factor $e^{-(\alpha/2)\tau}$, in which $\tau$ can be defined as the time order of the transient state. For example, if $\tau = 460$ for $\alpha = 0.02$ then $e^{-(\alpha/2)\tau} \sim 1\%$. Furthermore, the real physical time $t$ can be easily derived from the relation of $\tau = (4\pi M_s \gamma)t$. This yields the transient time $t = 2.4$ ns which is in good agreement with our simulation results shown in Fig. 3.

Figure 3(d) shows the phase difference of the final state $\phi_- = \phi_1 - \phi_2$ as a function of the injected current $I$, including both the prediction curve of the approximate theory (black line) and the simulation curves from macrospin (blue solid squares) and micromagnetic (red open squares) calculations. From the approximate theory, the stable phase difference for the softer (without $k$) phase-locking condition satisfies $-A_{disc}(d_{ee})\sin(\phi_-) - a_{J-} = 0$ and $|a_{J-}/A_{disc}(d_{ee})| < 1$. Therefore, the relationship between $\phi_-$ and $I$, and the maximum injected current for phase locking can be analytically obtained

$$\phi_- = \sin^{-1}\left[-\left(\frac{\hbar}{8\pi eM_S^2 V}\right)\frac{\Delta\varepsilon}{A_{disc}(d_{ee})}I\right],$$

$$|I| < \left(\frac{8\pi eM_S^2 V}{\hbar}\right)\frac{A_{disc}(d_{ee})}{|\Delta\varepsilon|}. \tag{14}$$

Here, $\Delta\varepsilon = \varepsilon_1 - \varepsilon_2$ with $P_1 = 0.38$, $P_2 = 0.44$, $\Lambda_1 = 1.8$, $\Lambda_2 = 2$, and $\theta_1 = \theta_2 = \pi/2$. Inserting all the parameters into Eq. (14), we obtain $\phi_- = \sin^{-1}[1.087 \times I]$,
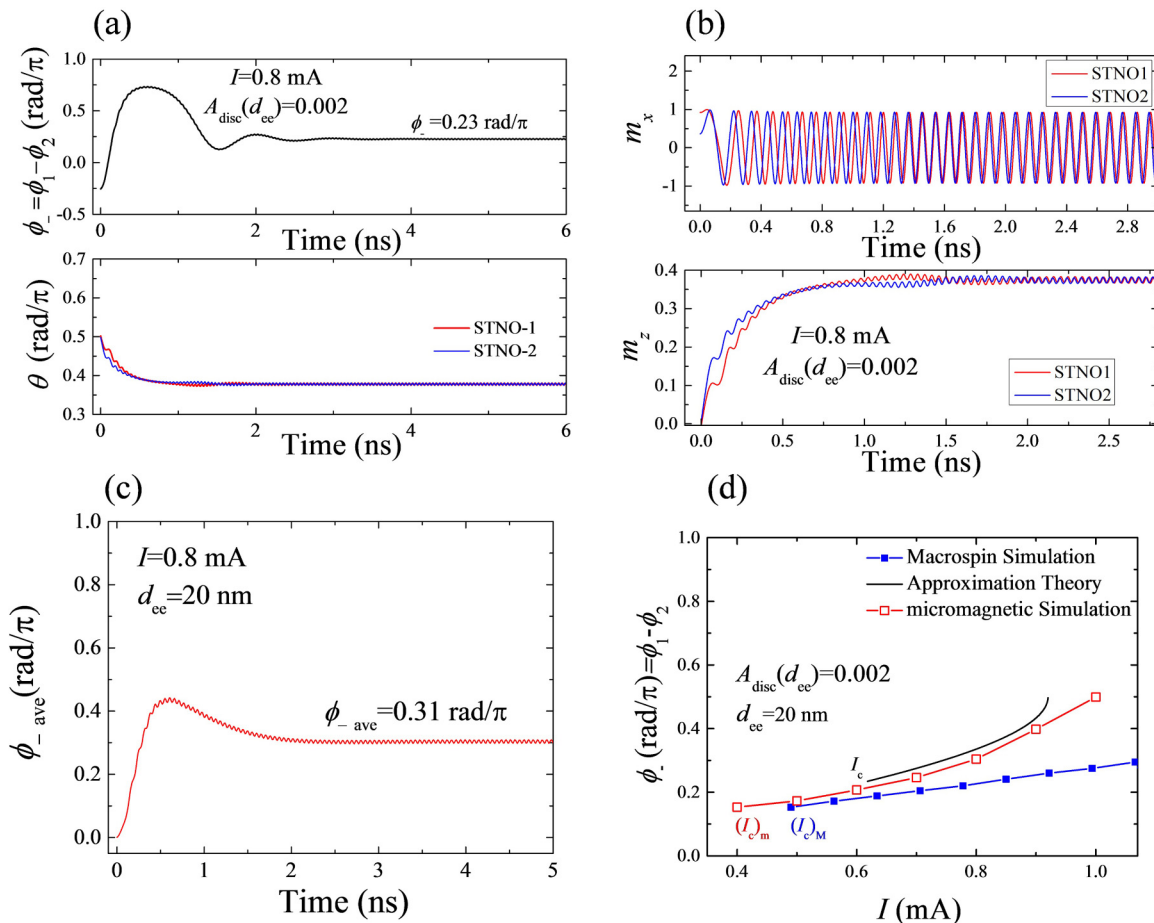
FIG. 3. The phase difference $\phi_- = \phi_1 - \phi_2$ and of the inclination angles $\theta_i$ for two nonidentical PERP STNOs. Macrospin simulations for (a) the time evolution of $\theta_i$ and the phase difference $\phi_-$ and (b) time evolution of the $x$ and $z$ components of the free-layer magnetization. The currents flowing through the STNO-1 and STNO-2 are 0.8 mA. The dipolar interaction strength is $A_{\mathrm{disc}}(d_{\mathrm{ee}}) = 0.002$. (c) Micromagnetic simulation for time evolution of $\phi_{-\mathrm{ave}}$. Here, $\phi_{-\mathrm{ave}}$ is the spatial averaged phase difference between the two free layers. (d) The current dependence of the phase difference $\phi_-$ calculated from different models: The black curve for the approximate theory, the blue solid squares for the macrospin simulation, and the red open squares for the micromagnetic simulations. $I_c = 0.618$ mA denotes the threshold current predicted by the approximation and $(I_c)_M = 0.5$ mA by the macrospin simulation.

$|I| < 0.92$ mA. It should be noted that the theoretical curve predicted by Eq. (14) is quite close to the macrospin and micromagnetic simulation results for the low-current case. In the high-current case, the $I$ dependence of $\phi_-$ predicted by the approximate theory is still quite close to the micromagnetic result, but a little different from the macrospin result. Interestingly, these results confirm that the angular profile of the disc dipolar coupling used in the approximation theory (see Appendix A) is quite reasonable. We would like to point out that the approximation theory is in principle valid only for precessions close to the thin film plane, i.e. for $\theta_i = \pi/2 + \delta\theta_i$ and $|\delta\theta_i| \sim \sqrt{k} \ll 1$, which corresponds to the case where the STT reaches its maximum magnitude when the free-layer magnetization lies in the plane of the film [19], but our calculations indicate that the dipolar coupling coefficient $A_{\mathrm{disc}}$ can still be used if $\theta = 0.34\pi = 61.54°$ for $I = 0.8$ mA.

Another interesting point is that the dependence of the phase difference $\phi_- = \phi_1 - \phi_2$ on current in Fig. 3(d) shows that the analytical curve is much closer to the micromagnetic simulation curve. We assume that unexpected behavior is caused by the fact that the analytical theory is in principle

only valid for the case of magnetization precession close to the film plane. At large currents, the phase difference can be enhanced in the analytical approximation by the fact that the high order terms of $\delta\theta$ in the expansion of the STT torque in Eqs. (B7) and (B8) have been eliminated. By contrast, in the micromagnetic simulation, due to the nonuniformity of the local magnetization configuration, the calculated dipolar coupling is actually smaller than that of the macrospin model in the high-current region. As a result, the phase difference in the micromagnetic simulation is enhanced at a large current when compared with the macrospin simulation.

The critical current to excite magnetization oscillation can be derived from Eq. (12a)

$$I_c = \left( \frac{8\pi e M_S^2 V}{\hbar} \right) \left[ \frac{3A_{\mathrm{disc}}(d_{\mathrm{ee}}) + k}{\varepsilon_1 + \varepsilon_2} \right]. \qquad (15)$$

Note that, in Fig. 3(d), the theoretical critical current is $I_c = 0.618$ mA, which is slightly larger than that of the macrospin (0.5 mA) and micromagnetic results (0.4 mA).
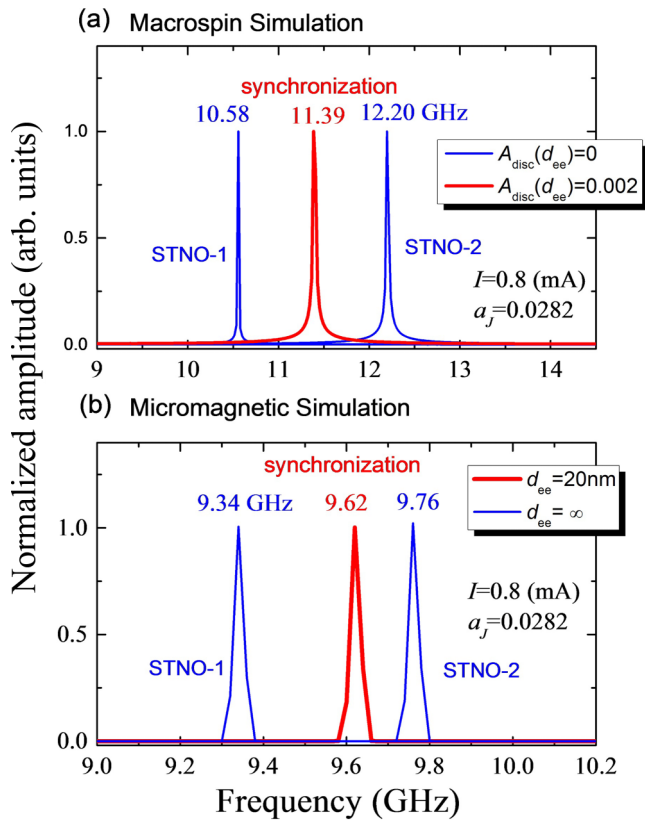
FIG. 4. Frequency spectra of the two nonidentical STNOs calculated by the FFT technique from the time evolution of $x$ components of the free-layer magnetization. The current is fixed to $I = 0.8$ mA for each STNO. (a) Macrospin simulations: The blue curves show the respective frequency of the two STNOs in the case without dipolar coupling; the red curve shows the frequency of the phase-locking state in the case with dipolar coupling. (b) Micromagnetic simulations: The blue curves show the respective frequency of the two STNOs without dipolar coupling, and the red curve shows the phase-locking frequency by the dipolar coupling.

## B. Frequency spectra of magnetization oscillations

The oscillation frequency can be calculated from the time evaluation of magnetization. Figures 4(a) and 4(b) show the oscillation frequency spectra for the STNO pair with (red curves) and without (blue curves) dipolar interaction effect simulated by the macrospin and the micromagnetic model, respectively. Here, the frequency spectra are calculated from the $x$ components through the fast Fourier transform (FFT) technique. The applied current for each STNO is 0.8 mA. Note that both the macrospin and micromagnetic simulations display two separate oscillation frequencies (blue curves) for the case without dipolar interaction between the two STNOs. This corresponds to the case where the separation $d_{ee} = \infty$ or $A_{disc}(d_{ee}) = 0$. The left STNO has a low frequency (10.58 GHz in macrospin and 9.34 GHz in micromagnetics) due to its relatively small spin-polarization efficiency ($P_1 = 0.38$, $\Lambda_1 = 1.8$), while the right STNO has a higher frequency (12.2 and 9.76 GHz for macrospin and micromagnetic simulations, respectively).

When the separation is decreased to 20 nm [i.e. $A_{disc}(d_{ee}) = 0.002$], the frequency of the STNO pair is locked at a medium
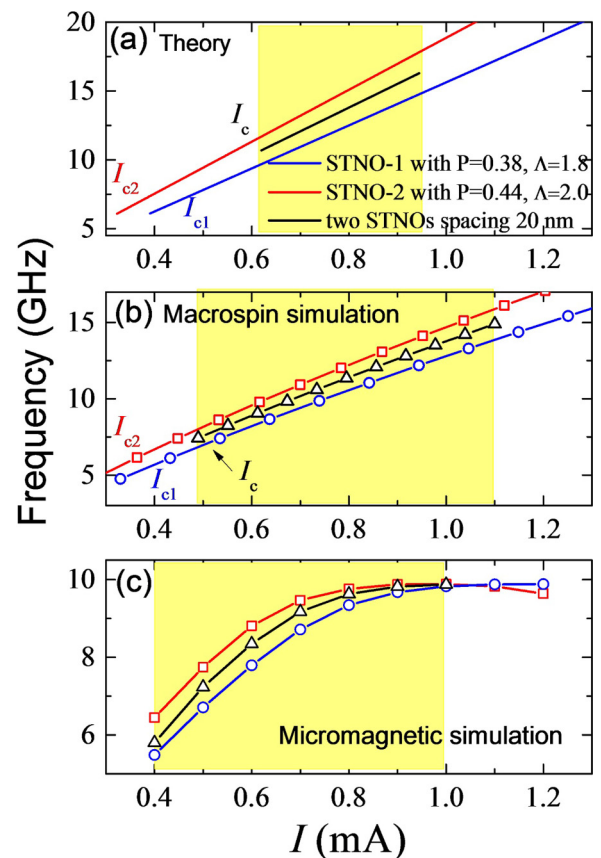


FIG. 5. Precession frequency of two nonidentical STNOs as a function of the current $I$ calculated from (a) approximation theory, (b) macrospin simulation, and (c) micromagnetic simulation. The red curves show the frequency for the STNO-1, the blue curves show the frequency for the STNO-2, and the black curves show the phase-locking frequency of the two STNOs through the dipolar coupling. The yellow background color regions show the current tunable range to achieve the phase-locking state. The threshold currents to excite precession states of STNO-1 and STNO-2 are indicated by $I_{c1}$ and $I_{c2}$, respectively. The threshold current for the phase-locking state of the two STNOs is marked by $I_c$.

value, 11.39 GHz in the macrospin simulation and 9.7 GHz in the micromagnetic simulations. This is shown by the red curves in Figs. 4(a) and 4(b). The synchronized frequency in the macrospin simulation is exactly located at the center of the two separated blue peaks, while in the micromagnetic simulation, there is a little shift to that of STNO-2. This result clearly confirms that, for a synchronized STNO pair, the magnetization of the two free layers precesses with the same angular velocity $\dot{\phi}$ as described by Eq. (13). The phase-locking angular velocity $\dot{\phi}$ is an average of the two original angular velocities $\dot{\phi}_{1,2}$.

Figure 5 shows the current tunable range of the phase-locking frequency in two nonidentical PERP STNOs. The macrospin simulations for the two STNOs with $P_1 = 0.38, \Lambda_1 = 1.8$ and $P_2 = 0.44, \Lambda_2 = 2$ are shown by the red and blue branches in Fig. 5(b). The critical driving current $I_c$ is around $0.3 \sim 0.4$ mA. This critical value $I_c$ can be estimated

from Eq. (5). From $|a_{J_{1,2}}| \geqslant k/2$, one obtains

$$a_{J01}\varepsilon_1(\theta_1 = \pi/2, P_1 = 0.38, \Lambda_1 = 1.8) \geqslant 0.008/2$$

$$a_{J02}\varepsilon_2(\theta_2 = \pi/2, P_2 = 0.44, \Lambda_2 = 2) \geqslant 0.008/2.$$

The calculated critical current for the left STNO is thus $I_{1c} = 0.39$ mA, and for the right one $I_{2c} = 0.323$ mA. We attribute the lower critical current in the right STNO to its relatively larger $P$. The right STNO therefore requires a relatively smaller current which can generate a strong enough STT to overcome the system barrier and then lead to a magnetization precession state. Note that, for current ranging from 0.4 to 1.2 mA, the macrospin simulation shows that the current dependence of the precessional frequency is linear [Fig. 5(b)], which is consistent with the prediction of the approximate theory [Fig. 5(a)]. Theoretically, an approximate relationship between current and frequency can be derived from Eq. (5) for a steady precession angular velocity $|\dot{\phi}_{1,2}| = |a_{J1,2}|/\alpha$,

$$
\begin{aligned}
f_{1,2}(\mathrm{GHz}) &= \frac{|a_{J1}|}{2\pi\alpha}(4\pi M_s\gamma) \\
&= \frac{\hbar(4\pi M_s\gamma)}{8\pi e M_s^2 V(2\pi\alpha)}\varepsilon_{1,2}(\theta, P, \Lambda)I_{1,2} \\
&= \begin{cases} 15.6 \times I_1(\mathrm{mA}) \\ 18.9 \times I_2(\mathrm{mA}) \end{cases}.
\end{aligned}
\tag{16}
$$

As we have mentioned before, the synchronization frequency of the two STNOs is an average value between their individual natural frequencies. From Eq. (14), the phase-locking frequency as a function of current is given by the black curve shown in Fig. 5(a). This result has been confirmed by both macrospin and micromagnetic simulations, as shown in Figs. 5(b) and 5(c). On the other hand, compared with individual STNO, it should be noticed that the critical current for the phase locking of the STNO pair increases due to the dipolar effect [Figs. 5(a) and 5(b)], as indicated in Eq. (12a). Note that, not only no synchronization is observed at a small current, but that the dipolar coupling effect will also fail to achieve the phase-locking state for a very large current. This is caused by the enhanced frequency difference between the two STNOs at an increased current [see Eq. (16)]. Our simulations indicate that the effective current of phase locking is 0.5–1.1 mA for the macrospin model and 0.4–0.8 mA for the micromagnetic model.

The phase-locking state of the two nonidentical STNOs precession strongly depends on the edge-to-edge distance $d_{ee}$ between the two nanopillars. This is due to the fact that the dipolar coupling decreases with increasing distance. Figure 6 shows the onset of phase locking as a function of the separation distance $d_{ee}$ for a given current $I = 0.8$ mA flowing through each nanopillar. Clearly, both the macrospin and the micromagnetic simulations show almost the same parameter range of the phase-locking state. The maximum edge-to-edge distance $(d_{ee})_M$ is ~20 nm. Below this critical value, the two STNOs have the same precessional frequency, implying that the dipolar coupling is strong enough to drive them into a phase-locked state. On the contrary, when the distance $d_{ee}$ is larger than this value, the two nonidentical STNOs lose phase,
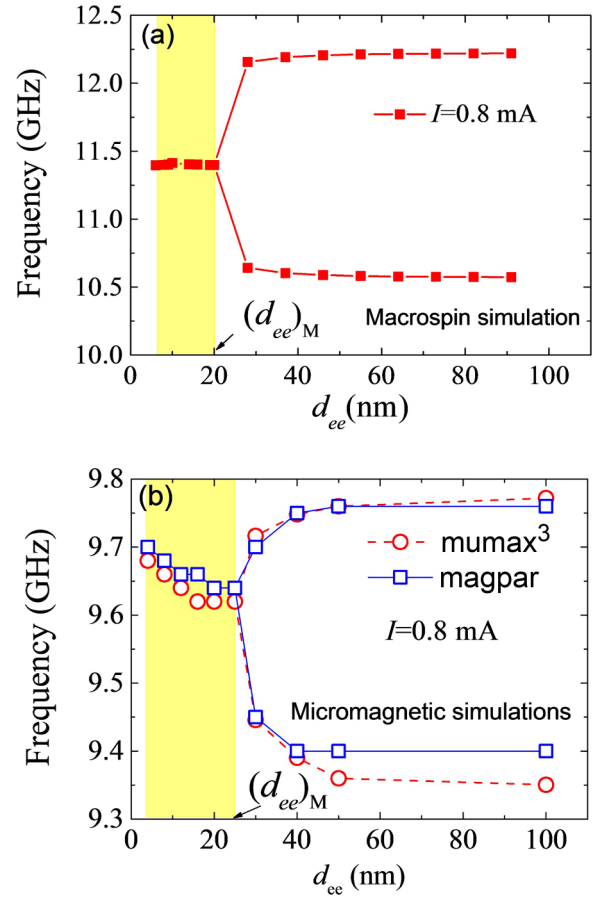


FIG. 6. Precession frequencies of two nonidentical STNOs as a function of the edge-to-edge distance $d_{ee}$. The injected current for each STNO is $I = 0.8$ mA. The yellow background color shows the parameter region of the phase-locking synchronization state. $(d_{ee})_M$ denotes the maximum edge-to-edge distance of the phase-locking state. (a) Macrospin simulation results. The dipolar coupling strength as a function of the edge-to-edge distance is taken from Fig. 10 in Appendix A. (b) Micromagnetic simulation results, in which the red and blue curves are results from the MuMax3 and magpar simulation codes, respectively.

and the frequency difference between them increases gradually with increasing distance $d_{ee}$, showing the decreased frequency in the left STNO, and the increased frequency in the right one.

Compared with the macrospin model, the locked frequency in the micromagnetic simulations increases gradually with the decrease of the separation $d_{ee}$. This interesting result can be attributed to the following: For a small separation (e.g. $d_{ee} = 4$ nm), the stray fields generated by the neighboring STNO slightly reduce the nonuniformity of the magnetization configuration. The increase of the uniform magnetization will in turn enhance the demagnetization fields. Therefore, the enhanced demagnetization field will increase the oscillation frequency.

## C. Phase-locking diagram

Finally, the phase diagrams of the two nonidentical STNO pairs as a function of distance and current are summarized in Fig. 7. The phase diagram is divided into three regions,
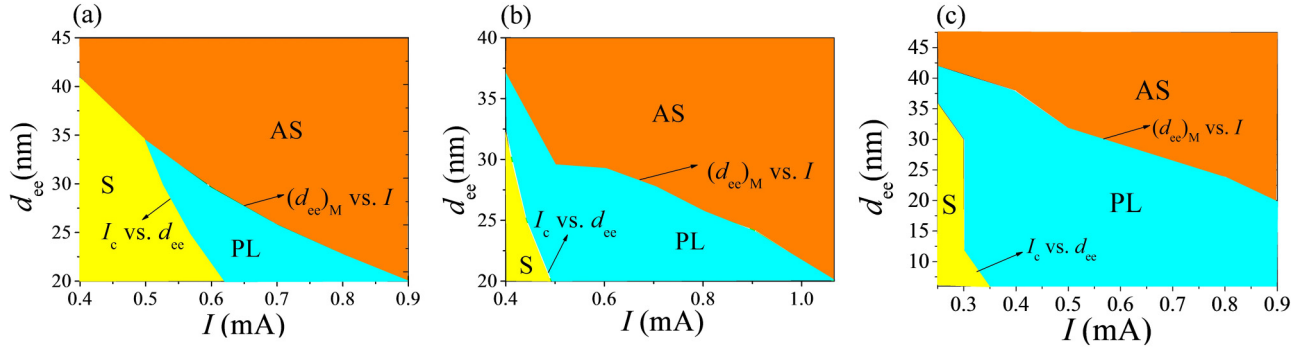
FIG. 7. Phase diagrams as a function of the edge-to-edge distance $d_{ee}$ and of the injected current $I$. (a) Prediction of the approximate theory. (b) Macrospin simulation. (c) Micromagnetic simulation. The central blue region represents the phase-locking (PL) mode. The yellow region is the steady (S) state without magnetization precession. The yellow region denotes the asynchronous (AS) precession mode. The border between the PL and AS states is separated by $(d_{ee})_M$.

including the steady state without magnetization precession (S state), the phase-locking precession state (PL state), and asynchronous state (AS state). The boundary between S and PL is the threshold current $I_c$, defined in Fig. 5. The boundary between the PL and AS states is the maximum edge-to-edge distance $(d_{ee})_M$, defined in Fig. 6. In the S state region, the current is too small to trigger the free-layer magnetization oscillation. In contrast, in the AS state region, the dipolar coupling between the two STNOs is not strong enough to drive a phase-locking state. From Fig. 7, one can see that the phase region of the approximation theory gives a good qualitative prediction with the numerical simulations, indicating that the dipolar coupling strength $A_{disc}(d_{ee})$ estimated from the assumption of uniformly magnetized thin film disc is quite reasonable for study of the phase-locking precession.

## IV. SUMMARY

We show that the magnetic dipolar coupling between PERP STNOs can be used as a driving force to synchronize a series of horizontally aligned nanopillar oscillators. In this paper, we have developed an approximate theory for two identical or nonidentical STNOs to predict their stable phase-locking state and the requisite parametric conditions. The theoretical predictions have been well confirmed qualitatively by macrospin and micromagnetic simulations. We calculated the relationship between the critical current of synchronization, the critical dipolar coupling strength, the phase-locking frequency, and the transient time as well. These results may open a starting point for the design of a reliable horizontal array of PERP STNOs phase locked through the dipolar coupling effect. This would represent an effective way to raise the output power of STNOs.

## ACKNOWLEDGMENTS

## APPENDIX A: APPROXIMATION THEORY FOR CALCULATION OF MAGNETIC DIPOLAR INTERACTION BETWEEN TWO CIRCULAR UNIFORMLY MAGNETIZED DISCS

As shown in Fig. 8, for two uniformly magnetized circular thin-film discs separated by an edge-to-edge distance $d_{ee}$, the magnetic dipolar interaction can be calculated via integrating the magnetostatic energy due to magnetic surface charges

$$A_{disc}\left(\frac{\pi}{2}, \phi_1, \frac{\pi}{2}, \phi_2\right) = \frac{1}{(4\pi M_s^2)V} \oint_{S_1} \oint_{S_2} \frac{(\sigma_1 dS_1)(\sigma_2 dS_2)}{\eta},$$
(A1)

Here, we assume that the magnetizations of the two discs are aligned in the film plane, i.e. $\theta_1 = \theta_2 = \pi/2$. The surface charge densities accumulated on the edges of two discs are written as $\sigma_1 = M_s \cos(\phi_1 - \phi')$ and $\sigma_2 = M_s \cos(\phi_2 - \phi'')$, where $\phi_1$ and $\phi_2$ are the $\phi$ coordinates of magnetizations, and $\phi'$ and $\phi''$ are the surface charge densities. The area elements $dS_1 = (Rd)d\phi'dz'$ and $dS_2 = (Rd)d\phi''dz''$, where $R$ is the radius of the discs. The distance between any pair of surface charges on the two discs is written as $\eta = \sqrt{[2R + d_{ee} + R(\cos\phi'' - \cos\phi')]^2 + [R(\sin\phi'' - \sin\phi')]^2 + (z'' - z')^2}$. In fact, when the edge-to-edge distance $d_{ee}$ is much larger than
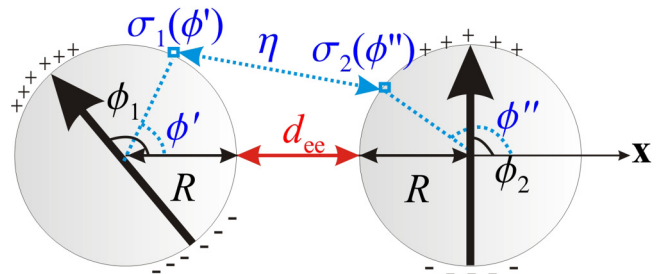


FIG. 8. A top view of two uniformly magnetized circular discs. The plus and minus signs represent the magnetic surface charge distributions $\sigma_1(\phi')$ and $\sigma_2(\phi'')$. $\phi'$ and $\phi''$ are the coordinates used to designate the locations of $\sigma_1$ and $\sigma_2$. $\eta$ is the distance between any pair of magnetic surface charges between the two discs. $\phi_1$ and $\phi_2$ are the magnetization directions, $R$ is the common radius of the two discs, and $d_{ee}$ is the edge-to-edge distance between them.

the disc thickness $d$, Eq. (A1) can be well approximated by calculating the magnetic interaction between two uniformly magnetized circle discs modeled by the inscribed regular $n$ polygons

$$A_{\text{disc}}\left(\frac{\pi}{2},\phi_1,\frac{\pi}{2},\phi_2\right) \approx \frac{1}{(4\pi M_s^2)V} \lim_{s,l\to\infty} \sum_{n=0}^{s-1}\sum_{m=0}^{l-1} \frac{q_{1n}q_{2m}}{\eta_{12}}. \tag{A2}$$

Here, the magnetic surface charges accumulated on the $n$th and $m$th edges of the two discs are given by $q_{1n} = M_s \cos(\phi_1 - \phi_n)\times 2R\sin(\frac{\pi}{l})\times d$ and $q_{2m} = M_s \cos(\phi_2 - \phi_m)\times 2R\sin(\frac{\pi}{s})\times d$. In these expressions, $l$ and $s$ denote the edge numbers of two regular $n$ polygons. The distance between the two charges has the form

$$\eta_{12} = \sqrt{\left[2R + d_{ee} + R\cos\left(\frac{\pi}{s}\right)\cos(\phi_m) - R\cos\left(\frac{\pi}{l}\right)\cos(\phi_n)\right]^2 + \left[R\cos\left(\frac{\pi}{s}\right)\sin(\phi_m) - R\cos\left(\frac{\pi}{l}\right)\sin(\phi_n)\right]^2}.$$

In order to analyze the phase-locking behavior from the point of view of dipolar interactions, a new set of variables $(\phi_+,\phi_-)$ are introduced to replace $(\phi_1,\phi_2)$. Note that, the form of the angular profile of $A_{\text{disc}}(\phi_+,\phi_-)$ is very similar to that of point dipolar interaction $A_{\text{point}}(\phi_+,\phi_-)$, especially in the locations of local energy maxima and minima, as shown in Fig. 9. However, when the distance $d_{ee}$ is smaller than 30 nm, the energy difference between local maxima and local minima of $A_{\text{disc}}(\phi_+,\phi_-)$ along $\phi_-$ direction is obviously larger than that of $A_{\text{point}}(\phi_+,\phi_-)$. This means that the dipolar coupling strength of two uniformly magnetization discs $A_{\text{disc}}(d_{ee})$ is larger than that of two point magnetic dipoles $A_{\text{point}}(d_{ee})$. This is because, when the magnetizations of two discs are placed in head-to-head or tail-to-tail configuration, they correspond to the local maximum of $A_{\text{disc}}(\phi_+,\phi_-)$, i.e. $|\phi_-| = \pi$. The magnetic energy comes mainly from the surface charges with the same sign, which are accumulated on the face-to-face edges of the two discs. The actual distance between any pair of magnetic charges is much smaller than the center-to-center distance $2R + d_{ee}$. Hence, for a smaller $d_{ee}$, the maximum dipolar interaction significantly grows with decreasing $d_{ee}$. Conversely, for configurations with local minimum of $A_{\text{disc}}(\phi_+,\phi_-)$, corresponding to the head-to-tail or tail-to-head configuration, the minimum dipolar interaction becomes significantly lower.

The energy difference between the local maxima and minima of $A_{\text{point}}(\phi_+,\phi_-)$ along $\phi_-$ is $A_{\text{point}}(d_{ee}) = V/4\pi(2R + d_{ee})^3$. Since $A_{\text{disc}}(\phi_+,\phi_-)$ is similar to $A_{\text{point}}(\phi_+,\phi_-)$, the disc dipolar field strength $A_{\text{disc}}(d_{ee})$ can be approximately estimated as the energy difference along $\phi_-$ between the local maxima and minima of $A_{\text{disc}}(\phi_+,\phi_-)$. Figure 10 shows the comparison of $A_{\text{disc}}(d_{ee})$ and $A_{\text{point}}(d_{ee})$. Obviously, the growth rate of $A_{\text{disc}}(d_{ee})$ is faster than that of $A_{\text{point}}(d_{ee})$ when $d_{ee}$ decreases.

## APPENDIX B: NEWTON-LIKE EQUATIONS

For the low-energy orbits with the total magnetic energy density $|G| \sim k > |G_{\text{dip}}| \sim A_{\text{disc}}(d_{ee})$, the orbits can be written as $[\theta_i(\tau),\phi_i(\tau)] = [\pi/2 + \delta\theta_i(\tau),\phi_i(\tau)](i = 1,2)$, where $|\delta\theta_i| \ll 1$. In the absence of damping and the STT effect, these orbits obey the energy conservation law $G_0(\pi/2,\pi/2,\phi_{01},\phi_{02}) = G_1(\pi/2 + \delta\theta_1,\pi/2 + \delta\theta_2,\phi_{11},\phi_{12})$, where $G_0$ and $G_1$ denote the energies of the initial and final states. By substituting Eqs. (3) and (4) into the energy conservation equation and expanding $(\delta\theta_i)^2$ on the

right-hand side, one can easily obtain

$$\frac{1}{2}\sum_{i=1}^{2}(\delta\theta_i)^2 \approx \frac{k}{2}\sum_{i=1}^{2}(\sin^2\phi_{0i} - \sin^2\phi_{1i}) + A_{\text{disc}}(d_{ee})$$
$$\times [(\sin\phi_{01}\sin\phi_{02} - 2\cos\phi_{01}\cos\phi_{02})$$
$$- (\sin\phi_{11}\sin\phi_{12} - 2\cos\phi_{11}\cos\phi_{12})]. \tag{B1}$$

Thus, the order of magnitude of $|\delta\theta_i| \sim \sqrt{k}$.

In the absence of Gilbert damping and the STT effect, by substituting $\theta_i = \pi/2 + \delta\theta_i$ into Eq. (2) and expanding it to the first order of $\delta\theta_i$, we obtain

$$\begin{cases} \delta\dot{\theta}_i = -\frac{\partial G}{\partial\phi_i} \\ \dot{\phi}_i = \frac{\partial G}{\partial\delta\theta_i} \end{cases}, \quad (i = 1,2). \tag{B2}$$

Here, the total energy density $G$ is

$$G(\delta\theta_1,\delta\theta_2,\phi_1,\phi_2) = \frac{1}{2}\sum_{i=1}^{2}\delta\theta_i^2 + \frac{k}{2}\sum_{i=1}^{2}\sin^2\phi_i + A_{\text{disc}}(d_{ee})$$
$$\times (\sin\phi_1\sin\phi_2 - 2\cos\phi_1\cos\phi_2). \tag{B3}$$

Note that $\delta\theta_i$ and $\phi_i$ in Eq. (B2) form a set of conjugate variables in the Hamiltonian formulation. Accordingly, an effective Hamiltonian can be defined as

$$H(\delta\theta_1,\delta\theta_2,\phi_1,\phi_2) = \frac{1}{2}\sum_{i=1}^{2}\delta\theta_i^2 + \frac{k}{2}\sum_{i=1}^{2}\sin^2\phi_i + A_{\text{disc}}(d_{ee})$$
$$\times (\sin\phi_1\sin\phi_2 - 2\cos\phi_1\cos\phi_2), \tag{B4}$$

and Eq. (B2) becomes

$$\begin{cases} \delta\dot{\theta}_i = -\frac{\partial H}{\partial\phi_i} \\ \dot{\phi}_i = \frac{\partial H}{\partial\delta\theta_i} \end{cases}, \quad (i = 1,2). \tag{B5}$$

We can obtain an effective Lagrangian by introducing the Legendre transformation $L(\phi_1,\phi_2,\dot{\phi}_1,\dot{\phi}_2) = \sum_{i=1}^{2}\dot{\phi}_i\delta\theta_i - H(\delta\theta_1,\delta\theta_2,\phi_1,\phi_2)$.

Thus, the effective Lagrangian is given by

$$L(\phi_1,\phi_2,\dot{\phi}_1,\dot{\phi}_2) = \frac{1}{2}\sum_{i=1}^{2}\dot{\phi}_i^2 - \frac{k}{2}\sum_{i=1}^{2}\sin^2\phi_i - A_{\text{disc}}(d_{ee})$$
$$\times (\sin\phi_1\sin\phi_2 - 2\cos\phi_1\cos\phi_2). \tag{B6}$$

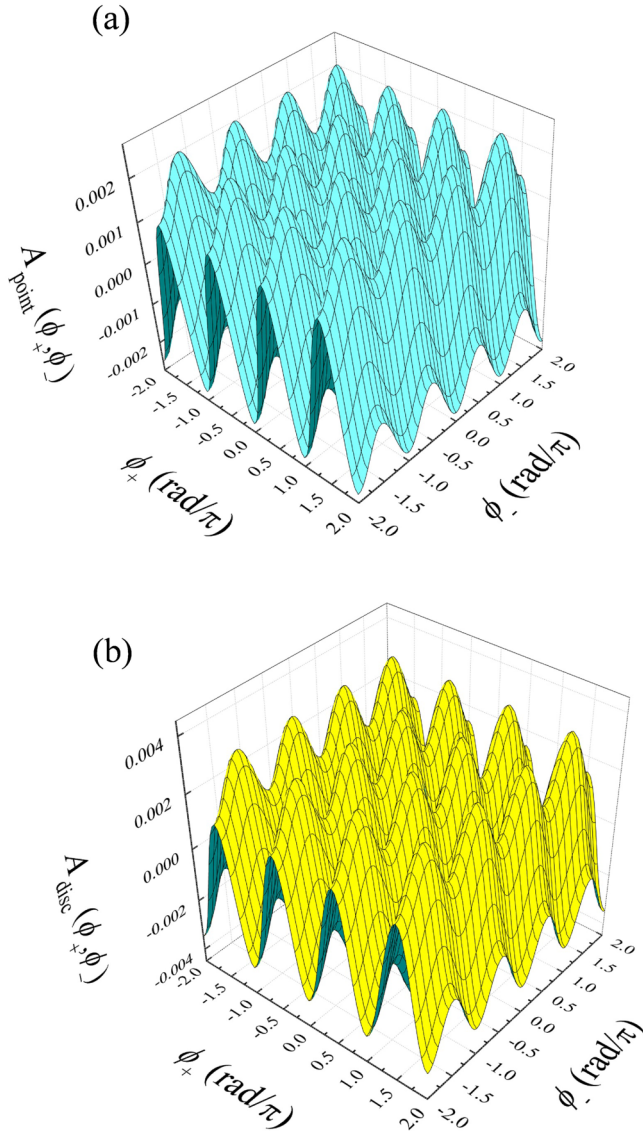The STT and the Gilbert damping torques are nonconservative effects, and we therefore need to construct it from the

(a)



(b)



FIG. 9. Magnetic dipolar coupling as a function of the phase sum and the phase difference $(\phi_+, \phi_-)$. The edge-to-edge distance $d_{ee}$ is 20 nm. The dipolar coupling profile is produced by two magnetic dipoles which are arranged (a) horizontally and (b) by two uniformly magnetized circular discs.

exact energy balance equation

$$\frac{dG}{d\tau} = \sum_{i=1}^{2} -\left[ \alpha \left| \frac{d\mathbf{m}_i}{d\tau} \right|^2 + a_{Ji}(\mathbf{m}_i)(\mathbf{m}_i \times \mathbf{p}) \cdot \frac{d\mathbf{m}_i}{d\tau} \right]. \quad \text{(B7)}$$

Under the low-energy approximation, $\theta_i = \pi/2 + \delta\theta_i$, $|\delta\theta_i| \sim \sqrt{k} \ll 1$, the energy Eq. (B7) can be approximated as

$$\frac{dG}{d\tau} \cong -\alpha \sum_{i=1}^{2} \left( \delta\dot{\theta}_i^2 + \dot{\phi}_i^2 \right) - \sum_{i=1}^{2} a_{Ji}\left(\theta_i = \frac{\pi}{2}\right)\dot{\phi}_i. \quad \text{(B8)}$$

For a low-energy orbit, the order of magnitudes of $|\dot{\phi}_i|$ and $|\delta\dot{\theta}_i|$ in Eq. (B2) can be estimated as

$$\begin{cases} \delta\dot{\theta}_i \sim -k, \quad (i=1,2) \\ \dot{\phi} \sim \sqrt{k}, \end{cases} \quad \text{(B9)}$$
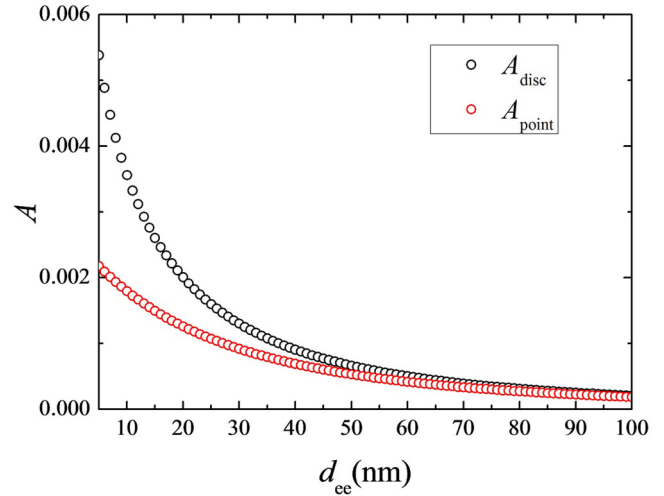


FIG. 10. The dependence of the dipolar coupling strength on the edge-to-edge distance $d_{ee}$. The red circles represent the strength produced by two magnetic dipoles in a horizontal array. The black circles represent the strength produced by two uniformly magnetized circular discs in a horizontal array.

Here, $|\dot{\phi}_i| \gg |\delta\dot{\theta}_i|$. Therefore, the energy balance equation can be further approximated in the form

$$\frac{dG}{d\tau} \cong -\alpha \sum_{i=1}^{2} \dot{\phi}_i^2 - \sum_{i=1}^{2} a_{Ji}\left(\theta_i = \frac{\pi}{2}\right)\dot{\phi}_i. \quad \text{(B10)}$$

Besides the damping effect, the contribution from the STT is also taken rigorously into account. We then can easily define an effective dissipation function in the Lagrangian dynamics

$$F_{\text{dis}} \equiv \frac{1}{2}\alpha \sum_{i=1}^{2} \dot{\phi}_i^2 + \sum_{i=1}^{2} a_{Ji}\left(\theta_i = \frac{\pi}{2}\right)\dot{\phi}_i. \quad \text{(B11)}$$

From the Euler-Lagrangian equations with dissipation, Eq. (5) is obtained.

Equation (5) is formally equivalent to

$$\begin{cases} \delta\dot{\theta}_i + \alpha\dot{\phi}_i + a_{Ji}\left(\theta_i = \frac{\pi}{2}\right) = -\frac{\partial G}{\partial \phi_i}, \\ \dot{\phi}_i = \frac{\partial G}{\partial \delta\theta_i}, \quad (i=1,2) \end{cases} \quad \text{(B12)}$$

and if the magnitudes of $|\delta\dot{\theta}_i|$, $|\dot{\phi}_i|$, $|\partial G/\partial \phi_i|$, and $|\partial G/\partial \delta\theta_i|$ are on the same order as those in Eq. (B2), then the necessary conditions for the validity of Eq. (5) are

$$\begin{cases} \alpha \leqslant \sqrt{k}, \\ \left| a_{Ji}\left(\theta_i = \frac{\pi}{2}\right) \right| \sim k, \quad (i=1,2) \end{cases} \quad \text{(B13)}$$

Finally, we would like to point out that a closely related analytical work by using Lagrangian approach was presented in Ref. [58], in which spin-wave normal modes have been studied in a single STT nanopillar device.

[1] J. C. Slonczewski, J. Magn. Magn. Mater. **159**, L1 (1996).

[2] L. Berger, Phys. Rev. B **54**, 9353 (1996).

[3] A. Slavin, Nat. Nanotech. **4**, 479 (2009).

[4] J. A. Katine and E. E. Fullerton, J. Magn. Magn. Mater. **320**, 1217 (2008).

[5] D. C. Ralph and M. D. Stiles, J. Magn. Magn. Mater. **320**, 1190 (2008).

[6] T. J. Silva and W. H. Rippard, J. Magn. Magn. Mater. **320**, 1260 (2008).

[7] B. Lenk, H. Ulrichs, F. Garbs, and M. Münzenberg, Phys. Rep. **507**, 107 (2011).

[8] Z. Zeng, G. Finocchio, and H. Jiang, Nanoscale **5**, 2219 (2013).

[9] H. S. Choi, S. Y. Kang, S. J. Cho, I.-Y. Oh, M. Shin, H. Park, C. Jang, B.-C. Min, S.-I. Kim, S.-Y. Park, and C. S. Park, Sci. Rep. **4**, 5486 (2014).

[10] S. I. Kiselev, J. C. Sankey, I. N. Krivorotov, N. C. Emley, R. J. Schoelkopf, R. A. Buhrman, and D. C. Ralph, Nature **425**, 380 (2003).

[11] A. M. Deac, A. Fukushima, H. Kubota, H. Maehara, Y. Suzuki, S. Yuasa, Y. Nagamine, K. Tsunekawa, D. D. Djayaprawira, and N. Watanabe, Nat. Phys. **4**, 803 (2008).

[12] A. V. Nazarov, H. M. Olson, H. Cho, K. Nikolaev, Z. Gao, S. Stokes, and B. B. Pant, Appl. Phys. Lett. **88**, 162504 (2006).

[13] D. Houssameddine, S. H. Florez, J. A. Katine, J.-P. Michel, U. Ebels, D. Mauri, O. Ozatay, B. Delaet, B. Viala, L. Folks, B. D. Terris, and M.-C. Cyrille, Appl. Phys. Lett. **93**, 022505 (2008).

[14] S. Urazhdin, V. Tiberkevich, and A. Slavin, Phys. Rev. Lett. **105**, 237204 (2010).

[15] K. J. Lee, O. Redon, and B. Dieny, Appl. Phys. Lett. **86**, 022505 (2005).

[16] D. Houssameddine, U. Ebels, B. Delaët, B. Rodmacq, I. Firastrau, F. Ponthenier, M. Brunet, C. Thirion, J.-P. Michel, L. Prejbeanu-Buda, M.-C. Cyrille, O. Redon, and B. Dieny, Nat. Mater. **6**, 447 (2007).

[17] J. H. Chang, H. H. Chen, and C. R. Chang, Phys. Rev. B **83**, 054425 (2011).

[18] B. Lacoste, L. D. Buda-Prejbeanu, U. Ebels, and B. Dieny, Phys. Rev. B **88**, 054425 (2013).

[19] M. Zhang, L. Wang, D. Wei, and K.-Z. Gao, J. Appl. Phys. **117**, 17D922 (2015).

[20] T. Devolder, A. Meftah, K. Ito, J. A. Katine, P. Crozat, and C. Chappert, J. Appl. Phys. **101**, 063916 (2007).

[21] W. Jin, Y. Liu, and H. Chen, IEEE. Trans. Magn. **42**, 2682 (2006).

[22] R. Adler, Proc. IRE **34**, 351 (1946).

[23] J. A. Acebrón, L. L. Bonilla, C. J. Pérez Vicente, F. Ritort, and R. Spigler, Rev. Mod. Phys. **77**, 137 (2005).

[24] S. Kaka, M. R. Pufall, W. H. Rippard, T. J. Silva, S. E. Russek, and J. A. Katine, Nature **437**, 389 (2005).

[25] F. B. Mancoff, N. D. Rizzo, B. N. Engel, and S. Tehrani, Nature **437**, 393 (2005).

[26] A. N. Slavin and V. S. Tiberkevich, Phys. Rev. B **74**, 104401 (2006).

[27] M. R. Pufall, W. H. Rippard, S. E. Russek, S. Kaka, and J. A. Katine, Phys. Rev. Lett. **97**, 087206 (2006).

[28] X. Chen and R. H. Victora, Phys. Rev. B **79**, 180402 (2009).

[29] V. Tiberkevich, A. Slavin, E. Bankowski, and G. Gerhart, Appl. Phys. Lett. **95**, 262505 (2009).

[30] V. Puliafito, G. Consolo, L. Lopez-Diaz, and B. Azzerboni, Physica B **435**, 44 (2014).

[31] T. Kendziorczyk, S. O. Demokritov, and T. Kuhn, Phys. Rev. B **90**, 054414 (2014).

[32] A. N. Slavini and P. Kabos, IEEE. Trans. Magn. **41**, 1264 (2005).

[33] A. Slavin and V. Tiberkevich, IEEE. Trans. Magn. **44**, 1916 (2008).

[34] A. Slavin and V. Tiberkevich, IEEE. Trans. Magn. **45**, 1875 (2009).

[35] J. Grollier, V. Cros, and A. Fert, Phys. Rev. B **73**, 060409 (2006).

[36] B. Georges, J. Grollier, V. Cros, and A. Fert, Appl. Phys. Lett. **92**, 232504 (2008).

[37] D. Li, Y. Zhou, B. Hu, and C. Zhou, Phys. Rev. B **84**, 104414 (2011).

[38] H. Chen, J. Chang, and C. Chang, SPIN **1**, 1 (2011).

[39] H.-H. Chen, C.-M. Lee, J.-C. Wu, L. Horng, C.-R. Chang, and J.-H. Chang, J. Appl. Phys. **115**, 134306 (2014).

[40] V. E. Demidov, S. Urazhdin, H. Ulrichs, V. Tiberkevich, A. Slavin, D. Baither, G. Schmitz, and S. O. Demokritov, Nat. Mater. **11**, 1028 (2012).

[41] V. E. Demidov, H. Ulrichs, S. V. Gurevich, S. O. Demokritov, V. S. Tiberkevich, A. N. Slavin, A. Zholud, and S. Urazhdin, Nat. Commun. **5**, 3179 (2014).

[42] A. Giordano, M. Carpentieri, A. Laudani, G. Gubbiotti, B. Azzerboni, and G. Finocchio, Appl. Phys. Lett. **105**, 042412 (2014).

[43] R. H. Liu, W. L. Lim, and S. Urazhdin, Phys. Rev. Lett. **110**, 147601 (2013).

[44] L. Liu, C.-F. Pai, D. C. Ralph, and R. A. Buhrman, Phys. Rev. Lett. **109**, 186602 (2012).

[45] M. Elyasi, C. S. Bhatia, and H. Yang, J. Appl. Phys. **117**, 063907 (2015).

[46] A. Ruotolo, V. Cros, B. Georges, A. Dussaux, J. Grollier, C. Deranlot, R. Guillemet, K. Bouzehouane, S. Fusil, and A. Fert, Nat. Nanotech. **4**, 528 (2009).

[47] A. D. Belanovsky, N. Locatelli, P. N. Skirdkov, F. A. Araujo, J. Grollier, K. A. Zvezdin, V. Cros, and A. K. Zvezdin, Phys. Rev. B **85**, 100409 (2012).

[48] S. Erokhin and D. Berkov, Phys. Rev. B **89**, 144421 (2014).

[49] F. Abreu Araujo, A. D. Belanovsky, P. N. Skirdkov, K. A. Zvezdin, A. K. Zvezdin, N. Locatelli, R. Lebrun, J. Grollier, V. Cros, G. de Loubens, and O. Klein, Phys. Rev. B **92**, 045419 (2015).

[50] Y. Liu, Z. Zhang, J. Wang, P. P. Freitas, and J. L. Martins, J. Appl. Phys. **93**, 8385 (2003).

[51] J.-H. Chang, H.-H. Chen, C.-R. Chang, and Y. Liu, Phys. Rev. B **84**, 054457 (2011).

[52] X. Li, Z. Zhang, Q. Y. Jin, and Y. Liu, New J. Phys. **11**, 023027 (2009).

[53] J. D. Jackson, *Classical Electrodynamics* (Hohn Wiley & Sons, Inc, Singapore, 2001).

[54] Y. Kuramoto, *Chemical Oscillations, Waves and Turbulence* (Springer, Berlin, 1984).

[55] W. Scholz, J. Fidler, T. Schrefl, D. Suess, R. Dittrich, H. Forster, and V. Tsiantos, Comput. Mater. Sci. **28**, 366 (2003).

[56] A. Vansteenkiste, J. Leliaert, M. Dvornik, M. Helsen, F. Garcia-Sanchez, and B. Van Waeyenberge, AIP Adv. **4**, 107133 (2014).

[57] F. Macià, F. C. Hoppensteadt, and A. D. Kent, Nanotechnol. **25**, 045303 (2014).

[58] G. Consolo, G. Gubbiotti, L. Giovannini, and R. Zivieri, Appl. Math. Comput. **217**, 8204 (2011).